Limits of Finite Element Methods in the Mid-Frequency Range

A. Hüppe[1], M. Kaltenbacher[1]

[1] *Alps Adriatic University, Klagenfurt, Austria, Email: andreas.hueppe@uni-klu.ac.at*

Introduction

In recent years, a variety of finite element methods (FEM) have been proposed to overcome some problems of the standard finite elements when dealing with acoustic computations in the time domain. We will focus on two higher order methods as well as on the h-FEM (mesh refinement). The hierarchical p-FEM and the standard h-FEM are applied to the wave equation and the spectral finite element method (s-FEM) to the conservation equations of acoustics. We will demonstrate the properties of the methods in terms of accuracy and efficiency by numerical test cases.

Governing Equations

In our contribution, the higher order spectral finite element method is applied to the conservation equations of acoustics given by

$$\frac{1}{\rho_0 c^2}\frac{\partial p'}{\partial t} + \nabla\cdot\vec{v}' = F\ , \tag{1}$$

$$\rho_0\frac{\partial \vec{v}'}{\partial t} + \nabla p' = 0\ . \tag{2}$$

In (1) and (2), $\vec{v}'$ denotes the acoustic velocity, p' the pressure, ρ_0 the density of the fluid and F a given source term.

On the other hand, we investigate the hierarchical p-FEM and h-FEM applied on the wave equation which reads as

$$\frac{1}{c^2}\frac{\partial^2 p'}{\partial t^2} - \Delta p' = f\ ;\ f = \frac{\partial F}{\partial t}\ . \tag{3}$$

The wave equation is derived from the acoustic conversation equations and the equations are valid for linear acoustic wave propagation.

FE basis functions

In the h-FEM, the accuracy of the solution is improved by choosing a finer mesh in the computational region while the unknowns are always approximated with (bi-)linear shape functions. Whereby the two higher order methods use higher order functions to improve the solution.

In the s-FEM the shape functions are Lagrange polynomials of order N

$$\mathcal{P}_j^N(\xi) = \prod_{i=0, i\neq j}^{N}\frac{\xi-\xi_i}{\xi_j-\xi_i}\ . \tag{4}$$

The supporting points of the functions are located at the zeros of the derivatives of Legendre polynomials. Furthermore the Gauss-Lobatto rule of order N is chosen for integration. This choice of shape functions and integration rule is referred to as the spectral element method. The fact that the location of integration points and supporting points of the polynomials coincide in this method has significant advantages which will be discussed later.

The p-FEM approximates the unknowns in terms of Legendre polynomials of order p and can be expressed by using Rodigues' formula

$$\mathcal{L}^p(\xi) = \frac{1}{2^p\ p!}\frac{\partial^p}{\partial\xi^p}\left(\xi^2-1\right)^p \tag{5}$$

Properties of this method and a detailed investigation is given in [7, 6].

Variational Formulation

The weak form of the wave equation can be obtained by a multiplication with a test function φ and integration by parts.

Find $p' \in H^1$ *such that*

$$\int_\Omega \frac{1}{c^2}\varphi\ \ddot{p}'\ \mathrm{d}\Omega + \int_\Omega \nabla\varphi\cdot\nabla p'\ \mathrm{d}\Omega = \int_\Omega \varphi\ f\mathrm{d}\Omega + \int_{\partial\Omega}\varphi\frac{\partial p'}{\partial n}\ \mathrm{d}\partial\Omega\ . \tag{6}$$

for all $\varphi \in H_0^1$.

Thereby, H^1 is the space of square integrable functions (also denoted by L^2), whose first order derivatives are also square integrable in a weak sense [1]. In order to obtain a stable finite element formulation for the conservation equations, the unknowns are thought to be defined in different Sobolev spaces. The weak form reads as:

Find $(\vec{v}', p') \in ([L^2]^d, H^1)$ *such that*

$$\frac{\partial}{\partial t}\int_\Omega \frac{1}{\rho_0 c^2}\ p'\ \varphi\ \mathrm{d}\Omega = \int_\Omega \vec{v}'\cdot\nabla\varphi\ \mathrm{d}\Omega - \int_{\partial\Omega}\varphi\ \vec{v}'\cdot\vec{n}\ \mathrm{d}\partial\Omega$$
$$\frac{\partial}{\partial t}\int_\Omega \rho_0\vec{\psi}\ \vec{v}'\ \mathrm{d}\Omega = -\int_\Omega \nabla p'\cdot\vec{\psi}\ \mathrm{d}\Omega \tag{7}$$

for all $(\vec{\psi}, \varphi) \in ([L^2]^d, H_0^1)$.

The spectral element discretization is done along with a Piola mapping as presented in [3]. According to [4] we define the discrete versions of the unknowns $\boldsymbol{p'} \in P_h^N$ and $\boldsymbol{v'} \in V_h^N$, where

$$P_h^N = \left\{\varphi_h \in H_0^1 \ \middle|\ \varphi_h|_{K_j}\circ\mathbf{F}_j \in \mathcal{P}_N\right\}\ ,$$
$$V_h^N = \left\{\boldsymbol{\psi}_h \in [L^2]^d \ \middle|\ |\det\mathcal{J}_j|\mathcal{J}_j^{-1}\boldsymbol{\psi}|_{K_j}\circ\mathbf{F}_j \in [\mathcal{P}_N]^d\right\}\ .$$

Functional Spaces

The functional space for the approximation of the acoustic pressure is the continuous Sobolev space H^1. The

acoustic particle velocity $\vec{v}'$ on the other hand is approximated in the discontinuous space L^2. This choice of spaces has tremendous effects on the numerical scheme. As an example we notice the location of the unknowns for a simple two element setup as shown in Figure 1. Furthermore, the discrete functional space V_h^N makes use

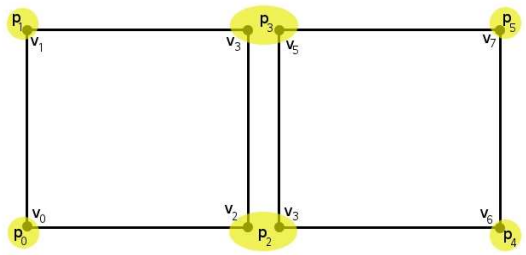

Figure 1: Locations of unknowns for the conservation equations

of a Piola mapping function for the finite elements. This definition results in the equality

$$\int_{\Omega_e} \nabla p' \cdot \boldsymbol{\psi} \mathrm{d}\Omega = \int_{\hat{\Omega}_e} \hat{\nabla} p' \cdot \hat{\boldsymbol{\psi}} \mathrm{d}\hat{\Omega} \,. \tag{8}$$

Therefore the stiffness integral can be evaluated for the reference element $\hat{\Omega}_e$ and applied to every element in the grid Ω_e.

Matrix System

The application of the finite element method to the wave equation yields the matrix equation for the homogeneous form

$$\mathbf{M}\ddot{\mathbf{p}}' + \mathbf{K}\mathbf{p}' = \mathbf{0} \,. \tag{9}$$

In (9), $\mathbf{M}$ denotes the mass matrix and $\mathbf{K}$ the stiffness matrix of the system.

For the conservation equation in homogeneous form we get the matrix equation system

$$\begin{pmatrix} \mathbf{D} & \mathbf{0} \\ \mathbf{0} & \mathbf{B} \end{pmatrix} \begin{pmatrix} \dot{\mathbf{p}}' \\ \dot{\mathbf{v}}' \end{pmatrix} = \begin{pmatrix} \mathbf{0} & \mathbf{R} \\ -\mathbf{R}^T & \mathbf{0} \end{pmatrix} \begin{pmatrix} \mathbf{p}' \\ \mathbf{v}' \end{pmatrix} \,, \tag{10}$$

where the mass matrices $\mathbf{D}$ and $\mathbf{B}$ are (block-)diagonal due to the use of the s-FEM. Therefore the application of explicit, non-dissipative time integration schemes is possible.

In the following, we use the leapfrog time integration scheme, which is second order accurate [8]. For the wave equation we apply an implicit Newmark integration scheme which in unconditionally stable and also features second order accuracy [5].

Numerical Examples

After the introduction of the numerical schemes the properties of both methods and their applicability in the mid-frequency range should be investigated by means of the following examples.

Convergence Analysis

As a first example the convergence of the space discretization should be investigated. Therefore we run a frequency domain computation of the setup pictured in Figure 2 for which an analytical solution is known. On the right hand

Figure 2: Setup of the pseudo 1D problem

side of the channel we choose $p' = 0$ and on the left hand side we apply a harmonic excitation signal with a given frequency f_0 and the corresponding wave number k_0. Initially, eleven elements per wavelength ($k_0 = 0.5$) are used for the discretization. Afterwards, the wave number is increased and the performance of the three methods is investigated. Figure 3 displays the accumulated error of h-FEM with respect to the analytical solution, where the increase of accuracy is achieved by a finer discretization of the domain. In difference to the linear convergence

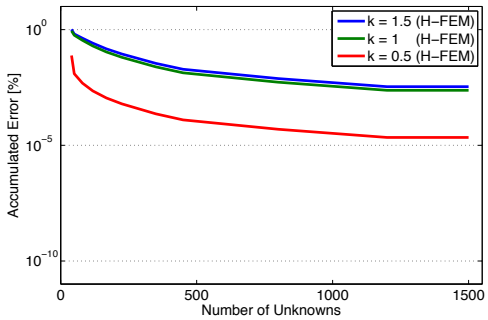

Figure 3: Convergence of h-FEM

property of h-FEM, the exponential convergence of p-FEM and s-FEM can be seen in Figure 4. It is visible

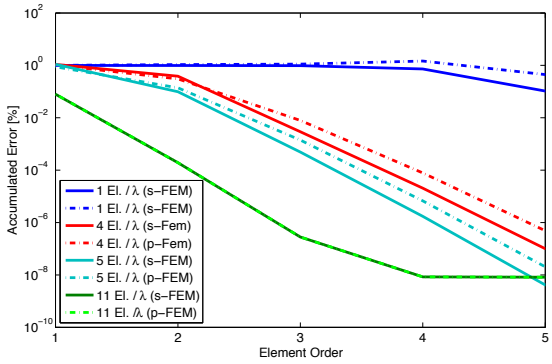

Figure 4: Convergence of p-FEM and s-FEM

that only the higher order finite element methods show a good behaviour for coarse discretizations. In case of one element per wavelength the non-convergence is caused by the dispersion relation shown in [6]. But if the element order is further increased, the same exponential convergence can be obtained.

This result is of particular interest when dealing with large scale problems in combination with higher frequencies. In this case, a mesh refinement (h-FEM)

would cause too much computational effort to obtain an accurate solution. Therefore we focus on the higher order methods in the following test cases.

Computation in Time Domain

To investigate the transient behaviour of the methods we choose the setup as pictured in Figure 5. On a

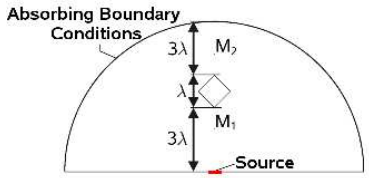

Figure 5: Setup for time domain computation

line (length $\approx \lambda_{\text{ref}}/4$) located at the bottom center of the domain a sine pressure pulse of frequency f_0 is applied as boundary condition. The obstacle was inserted to generate a more complicated sound field at the monitoring point M_2 thus making the properties of s-FEM and p-FEM more obvious. The signal at the monitoring point is afterwards compared to a reference solution obtained with a very fine discretization in space and time ($h_{\text{ref}} \approx \lambda_0/120$, $\Delta t_{\text{ref}} < 1/(f_0\ 200)$).

We choose absorbing boundary conditions (ABC) on the outer arc which can be found for the wave equation e.g. in [5]. For the conservation equations, the ABC is incorporated by an evaluation of the boundary integral using the relation $\vec{v}' \cdot \vec{n} = (1/Z_a)p' = 1/(\rho_0 c)p'$ [2]. This yields the relation

$$\int_{\partial\Omega} \varphi\ \vec{v}' \cdot \vec{n}\ \mathrm{d}\vec{x} = \int_{\partial\Omega} \frac{1}{Z_0} \varphi\ p'\ \mathrm{d}\vec{x}\ . \qquad (11)$$

For the simulations with higher order methods a much coarser discretization with about five elements per wavelength is used along with a free mesh as shown in Figure 6. The time step size for the simulations is chosen to

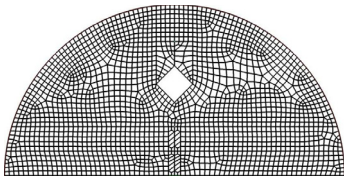

Figure 6: Free mesh for higher order computations

be one half of the limiting CFL-condition for the explicit leapfrog scheme used in the s-FEM. Shown in Figure 7 is the signal at M_2 for both methods in comparison to the reference solution. Clearly visible are the differences in the signals. The variances in the p-FEM solution are most likely caused by the implicit time stepping method when dealing with pulse excitations. A decrement of the time step size and increasing the element order shows also good convergence for the p-FEM.

Broadband Computation in Time Domain

More interesting in practical applications is the behaviour of the methods when dealing with larger fre-

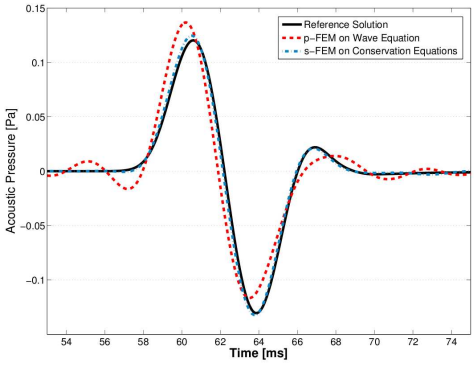

Figure 7: Signal at M_2 with order 3 elements

quency ranges. To illustrate this, we choose the two dimensional setup as pictured in Figure 8. The input

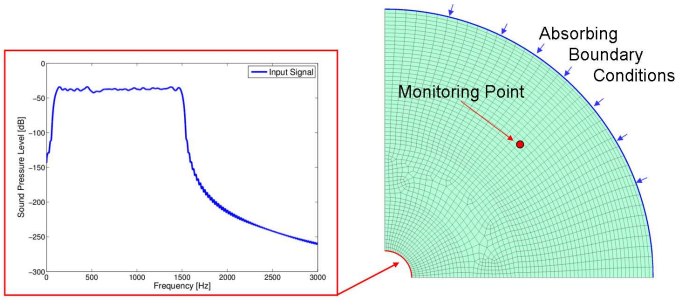

Figure 8: Computational setup and frequency spectrum of the transient input signal

signal is randomly generated and then filtered to have a banded spectrum. The upper frequency limit is $f_{\max} = 1500$Hz and the lower limit is set to $f_{\min} = 200$Hz. The edge lengths of the elements in the mesh vary in the range $\lambda_{\max}/3.5 < h < \lambda_{\max}$ and the resulting mesh has therefore 2096 elements. We choose a very fine time discretization ($\Delta t \leq 1/(100 f_{\max})$) to eliminate the error due to temporal integration and compute 10000 time steps. The monitoring point is defined 7 m away from the excitation surface and the outer radius of the domain is chosen to be 10 m.

For the p-FEM the spectra of the input signal and the received signal for first and fifth order elements is pictured in Figure 9. It can be seen, that the first order

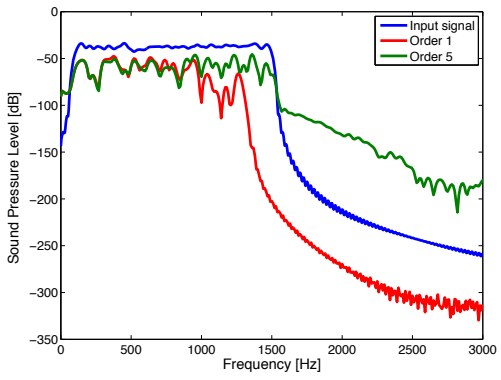

Figure 9: Frequency spectrum obtained by the p-FEM

element approximation already seems to cover a wide frequency range but a closer look at the time signal shows its heavy distortion. The usage of the fifth order element on the other hand covers the complete frequency range. The runtime of the fifth order simulation was about half an hour on a desktop PC (quad-core CPU,2.5GHz with 8GB RAM).

The results obtained by s-FEM is shown in Figure 10. It is visible that the mesh is basically too coarse for the use of lower order elements in the context of conservation equations. For the higher order approximation the frequency range was completely transmitted over the mesh quite similar to the results obtained by p-FEM. But its also visible that higher frequencies appear in both

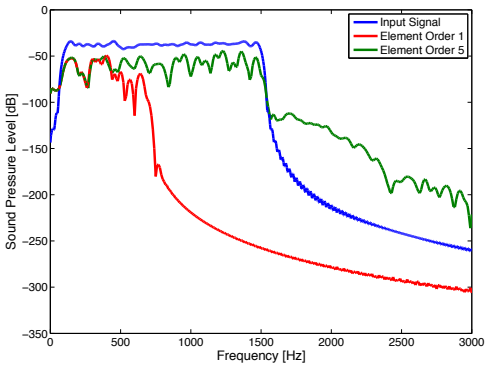

Figure 10: Frequency spectrum obtained by the s-FEM

spectra which are not included in the input signal. When choosing a finer discretization in space and time these components can be avoided. Nevertheless their SPL is about 50dB below the wanted signal thus having only minor impact on the transient signal.

For this setup, the required computational resources should be investigated to clarify the practical applicability of the methods. Pictured in Figure 11 is the computational time required for a simulation run with $N_t = 5000$ time steps. We compare here the com-

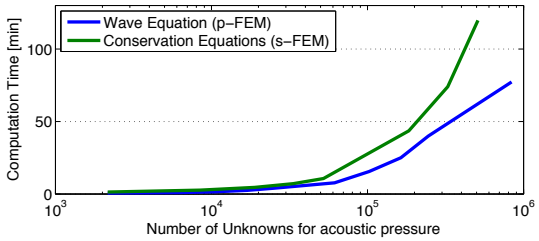

Figure 11: Runtime of a simulation $N_t = 5000$

putational time with respect to the pressure unknowns disregarding the velocity unknowns in the case of s-FEM solving the conservation equations. Even though the overall number of unknowns in the system is significantly higher the computational time still remains in the range of the p-FEM case. This behaviour is caused by the special matrix structures and the application of explicit time stepping schemes which enable the implementation of very efficient algorithms.

Also interesting is the memory consumption of the simulation. The memory requirement with respect to the overall number of unknowns is shown in Figure 12. It can be seen that s-FEM applied to the conservation equations is very efficient in its memory consumption.

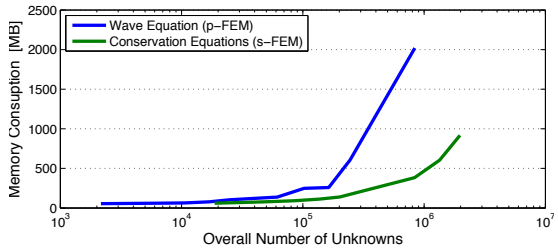

Figure 12: Memory consumption of the simulation run

Conclusion

We have shown, that field methods are applicable for simulations in the mid-frequency range, if we make use of higher order finite element methods. Also the high accuracy and good performance of both methods has been shown. Especially the spectral element method is a very interesting approach. On the one hand it is a very efficient method in memory consumption and on the other hand its computational time is comparable to the p-FEM even though the equation systems are significantly larger. It is one major topic of the authors research to optimize the implementation of the method, extend it towards acoustic impedance conditions in the time domain and investigate its applicability to aeroacoustic problems.

References

[1] R. Adams. *Sobolev Spaces*. Pure and Applied Mathematics. Academic Press, 1975.

[2] D. T. Blackstock. *Fundamentals of Physical Acoustics*. Blackstock, 2000.

[3] F. Brezzi and M. Fortin. *Mixed and Hybrid Finite Element Methods*. Springer, New York, 1991.

[4] G. Cohen and S. Fauqueux. Mixed finite elements with mass-lumping for the transient wave equation. *Journal of Computational Acoustics*, 8:171 – 188, 2000.

[5] M. Kaltenbacher. *Numerical Simulation of Mechatronic Sensors and Actuators*. Springer, Berlin, 2. edition, 2007.

[6] M. Kaltenbacher, A. Hauck, and R. Lerch. Hierarchische finite-elemente für die numerische berechnung von akustischen feldproblemen. In *Proceedings of the DAGA'07*, 2007.

[7] B. Szabó and I. Babuška. *Finite Element Analysis*. John Wiley & Sons, Inc., 1991.

[8] W. Zhou. An alternative leapfrog scheme for surface gravity wave equations. *Journal of Atmospheric and Oceanic Technology*, 19(9):1415–1423, 2002.